

Universal conductance fluctuations in Dirac semimetal Cd₃As₂ nanowires

Li-Xian Wang,¹ Shuo Wang,¹ Jin-Guang Li,¹ Cai-Zhen Li,¹ Dapeng Yu,^{1,2,3} and Zhi-Min Liao^{1,4,*}

¹State Key Laboratory for Mesoscopic Physics, School of Physics, Peking University, Beijing 100871, People's Republic of China

²Electron Microscopy Laboratory, School of Physics, Peking University, Beijing 100871, People's Republic of China

³Department of Physics, South University of Science and Technology of China, Shenzhen 518055, China

⁴Collaborative Innovation Center of Quantum Matter, Beijing 100871, People's Republic of China

(Received 6 May 2016; published 14 October 2016)

Three-dimensional Dirac semimetals host bulk Dirac fermions characterized by a linear dispersion relation in momentum space along all three dimensions. It has been theoretically predicted that the breaking of C_4 rotational crystalline symmetry in the Dirac semimetal Cd₃As₂ may give rise to the massive Dirac fermions. Here we report the phase-coherent transport in Cd₃As₂ nanowires studied by measuring the universal conductance fluctuations (UCFs). It is found that the UCF amplitude is largely suppressed at the Dirac point by sweeping the magnetic field at different gate voltages, which is ascribed to the breaking of the C_4 rotational symmetry-induced band-gap opening. The temperature dependence of resistance demonstrates a magnetic-field-induced metal-insulator transition, consisting of the band-gap opening. Moreover, the UCF amplitude is reduced by a factor of $\sim 2\sqrt{2}$ in the presence of a magnetic field, suggesting the phase transition from a Dirac-to-Weyl semimetal by breaking time-reversal symmetry.

DOI: [10.1103/PhysRevB.94.161402](https://doi.org/10.1103/PhysRevB.94.161402)

Three-dimensional (3D) Dirac semimetals have attracted increasing attention due to their linear energy band dispersion relations along all three momentum directions [1–7]. The large Fermi velocity near the Dirac points facilitates the massless Dirac fermions with high mobility [8,9]. By breaking time-reversal symmetry or inversion symmetry, the degenerate Dirac point splits into a pair of Weyl points separated in the momentum space, leading to a transition from Dirac to Weyl semimetals [2,3,10]. Moreover, the breaking of rotational crystalline symmetry is theoretically predicted to open a gap at the Dirac point [3,11–13]. In Dirac semimetal Cd₃As₂, magnetotransport measurements have been carried out to reveal the unique properties of the Dirac fermions [8,9,14–16] and the chiral anomaly effect related to the Weyl fermions in the low-energy dispersion [17–20]. As demonstrated in graphene and topological insulators [21,22], the quantum interferences are investigated to reveal the eigenvalue degeneracy with an underlying mechanism. Scaling down to the phase-coherent region, the quantum correction ΔG_Q to classical conductance becomes remarkable and manifests itself in distinct forms, such as weak antilocalization (WAL), the Aharonov-Bohm effect, and the Altshuler-Aronov-Spivak effect in Dirac semimetals [17,23,24]. Universal conductance fluctuations (UCFs) are a consequence of quantum interferences among all the phase-coherent trajectories and are featured as repeatable fluctuations of conductance. The amplitude of UCFs is related to the phase-coherence length L_ϕ , the sample size L , and the symmetry of the Hamiltonian, which offers deeper insight into the quantum transport properties [25,26]. In the presence of strong spin-orbit coupling, the WAL effect has been observed in Cd₃As₂, indicating that the phase coherence in quantum interferences can be maintained within hundreds of nanometers [23]. To explore rich quantum phenomena aside from the WAL effect, we were motivated to reduce the size of the device down to $L < L_\phi$. In these short-channel devices,

our studies demonstrate that the phase-coherent transport can be realized in the entire transport channel of the Cd₃As₂ nanowire, which is important for the design of the functional device based on the Dirac semimetal system with sizes down to the nanoscale.

Here we report systematic measurements of the UCF in Dirac semimetal Cd₃As₂ nanowires. The employment of gate modulation allows us to study the transport behaviors around the Dirac point. Detailed analysis on UCF patterns reveals the magnetic-field-induced band-gap opening at the Dirac point and the breaking of time-reversal symmetry-induced splitting of the Dirac point.

The Cd₃As₂ nanowires were synthesized by the chemical-vapor deposition method (CVD) [17]. The nanowires with single-crystalline nature grew along the [110] direction as represented in the high-resolution transmission electron microscopy image in Fig. 1(a). By the CVD method, we were able to obtain Cd₃As₂ nanowires with a [110] or [112] growth direction, depending on the growth temperature T_g . Specifically, we obtained the [110] nanowires at $T_g = 700^\circ\text{C}$ and the [112] nanowires [17] at $T_g = 650^\circ\text{C}$. The Cd₃As₂ nanowire devices were fabricated on a Si substrate with a 285-nm SiO₂ layer. As shown in Fig. 1(b), a typical device has multiple Au (100-nm)/Ti (5-nm) electrodes that form ohmic contacts with the Cd₃As₂ nanowire. The measurement configuration is schematically shown in the inset of Fig. 1(c). The transport measurements were performed in an Oxford cryostat system with a variable temperature insert, and the electrical signals were measured using a four-terminal method using lock-in amplifiers at a frequency of 17.7 Hz. The magnetic field was applied perpendicular to the substrate in the measurements. By employing a backgate on the Si substrate, we were able to modulate the Fermi level of the Cd₃As₂ nanowire directly by tuning the backgate voltage V_g .

Figure 1(c) shows the transfer curve of a nanowire device with a diameter of $D \sim 100\text{ nm}$ and a channel length of $L \sim 600\text{ nm}$. The ambipolar field effect with a minimum conductance at $V_g \sim 20\text{ V}$ is observed. From the V_g depen-

*liaozm@pku.edu.cn

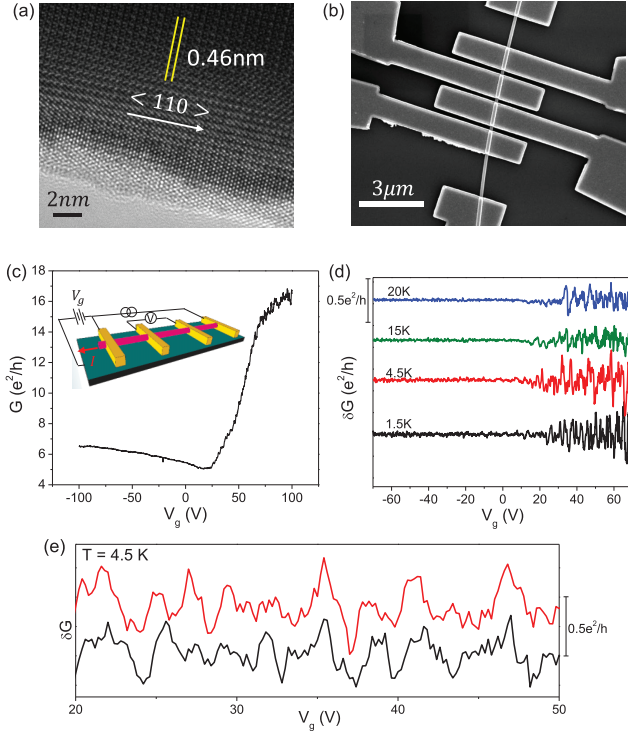


FIG. 1. (a) High-resolution transmission electron microscopy image of a typical nanowire with an interplanar space of ~ 0.46 nm in the $\langle 110 \rangle$ growth direction. (b) Scanning electron microscopy image of a typical nanowire-based device with multiple terminals. (c) The transfer curve exhibits a single minimum in conductance as tuning the backgate voltage V_g , suggesting the ambipolar field effect. The electrical circuit for standard four-terminal measurements is schematically shown in the inset. (d) Extracted fluctuations δG from transfer curves by careful subtraction of the gate-tunable background at different temperatures. (e) Repeatable conductance fluctuations of two subsequent forward sweeps of the gate voltage at 4.5 K.

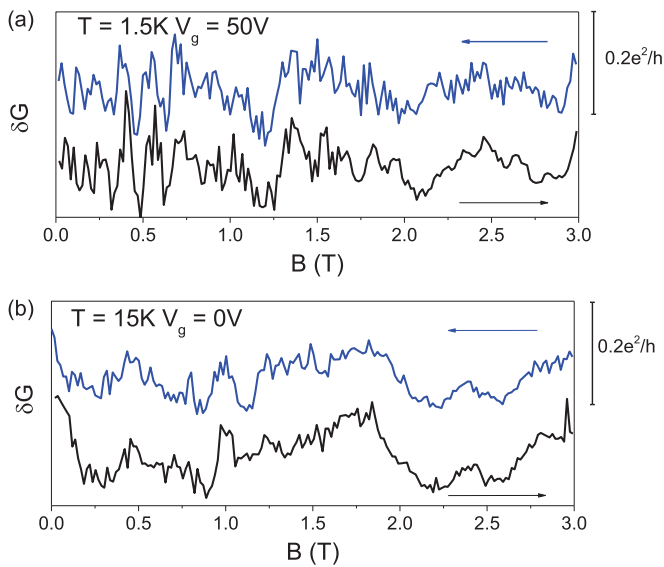


FIG. 2. Repeatable conductance fluctuations as forward and backward sweeping magnetic fields at (a) $T = 1.5$ K and $V_g = 50$ V and (b) $T = 15$ K and $V_g = 0$ V. The sweep direction is denoted by the arrow.

dence of the channel conductance G , the carrier mobility is estimated to be $\mu_e = 1630 \text{ cm}^2 \text{ V}^{-1} \text{ s}^{-1}$ for electrons and $\mu_h = 117 \text{ cm}^2 \text{ V}^{-1} \text{ s}^{-1}$ for holes. Noticeably, the conductance manifests aperiodic fluctuations in the electron conduction branch as shown in Fig. 1(d). As the dimension of the devices is comparable to the phase-coherence length L_ϕ , the quantum interference effect will result in the UCFs. Using V_g to tune the Fermi-level E_F and thus the Fermi-wave-vector k_F , the interference pattern can be modulated due to the phase changes between phase-coherent trajectories, leading to the conductance fluctuations that keep consistency between subsequent measurements [Fig. 1(e)]. Figure 1(d) shows that the amplitude of fluctuations enhances dramatically as the Fermi level is high above the Dirac point, which is consistent with the fact that the electron mobility is much higher than that of the hole. It is also found that the root-mean square (rms) of conductance fluctuations δG_B^{rms} decreases with increasing temperature. The δG_B^{rms} is $0.0958e^2/h$ at 1.5 K, whereas it reduces to $0.0423e^2/h$ at 20 K. The temperature dependence of δG_B^{rms} is consistent with the quantum origin of UCFs,

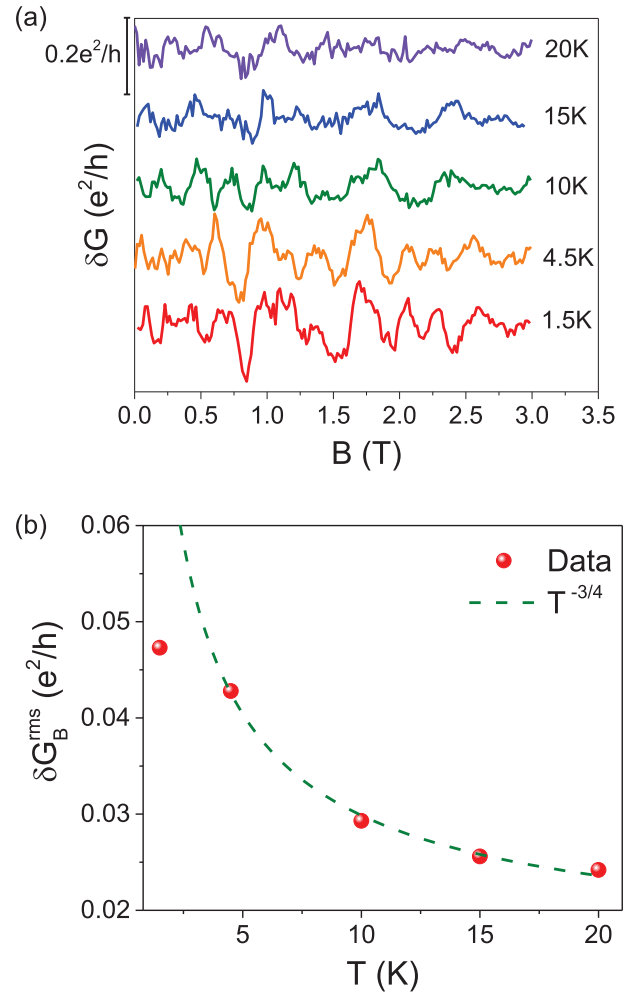


FIG. 3. (a) Extracted fluctuations δG from magnetoconductance $G(B)$ at a positive gate voltage of $V_g = 52$ V from 1.5 to 20 K. The curves are vertically shifted for clarity. (b) Calculated rms of fluctuation δG in (a) at different temperatures T , demonstrating the $T^{-3/4}$ power-law dependence.

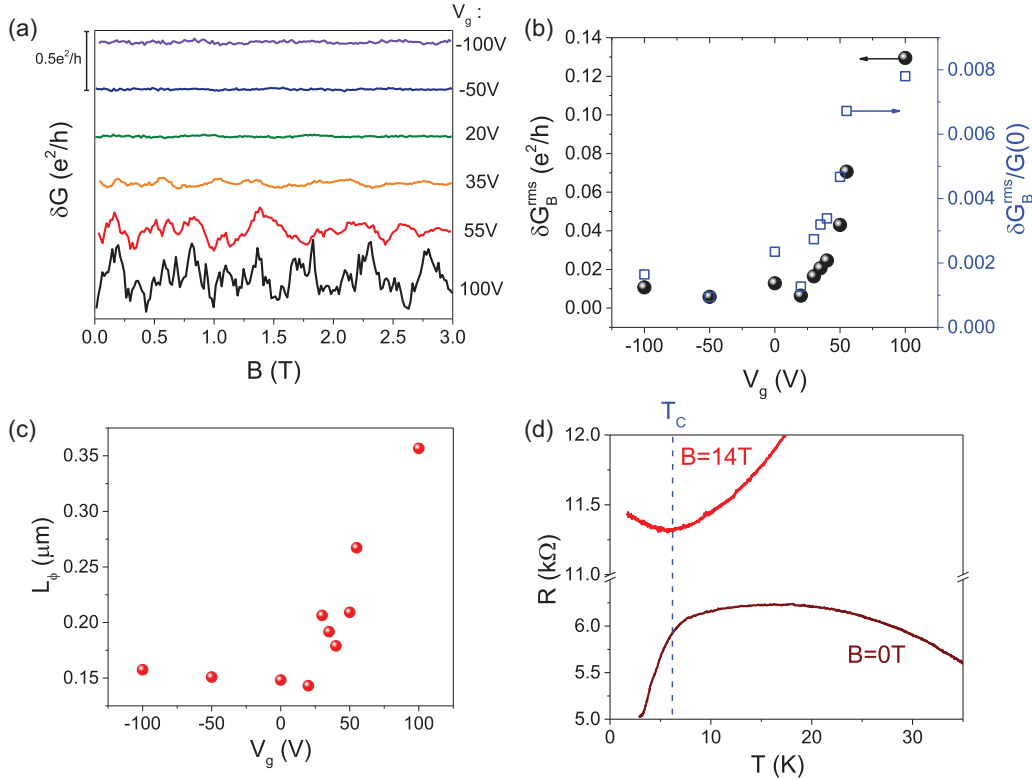


FIG. 4. (a) The conductance fluctuations δG as a function of the magnetic field at different gate voltages. (b) The δG_B^{rms} and $\delta G_B^{rms}/G(0)$ as a function of the gate voltage. (c) The calculated coherence length L_ϕ as a function of the gate voltage. (d) The temperature dependence of resistance under $B = 0$ and 14 T.

suggesting the thermal-induced reduction of the coherence length L_ϕ .

The UCFs were further investigated by altering the phase of the electron wave by the magnetic field. Upon sweeping of the magnetic field, the conductance exhibits evident aperiodic oscillations at $T = 1.5$ K and $V_g = 50$ V as shown in Fig. 2(a). The main features are almost reproducible as forward and backward sweeping the magnetic field, giving evidence that the repeatable fluctuation δG should not be from random noise. Further increasing the temperature to 15 K, the reproducible UCF patterns are still clearly observed even at $V_g = 0$ V as shown in Fig. 2(b). The changes in the magnetic flux enclosed by all the possible paths result in the conductance fluctuations. In order to investigate the temperature dependence of the UCFs, the δG as a function of the magnetic field at different temperatures was measured in the electron conduction regime with high carrier mobility at $V_g = 52$ V, and the results are presented in Fig. 3(a). The trace of fluctuation δG at 1.5 K almost coincides with that at 4.5 K, indicating the nature of the quantum interference effect. As the temperature increases to 10 K, the thermal activation becomes considerable and induces the change in carrier concentration and the Fermi-level E_F . It gives rise to the variation of Fermi-vector k_F , thus leading to distinct fluctuation patterns at 10 K from those at 1.5 K. Further insight into the fluctuation pattern can be obtained by analyzing the autocorrelation function $F(\Delta B) = \frac{\langle \delta G(B) \delta G(B + \Delta B) \rangle_B}{\langle \delta G^2 \rangle}$, where $\langle \dots \rangle_B$ is the average with respect to magnetic-field B (Ref. [25]). The correlation field B_0 can be obtained via $F(B_0) = 0.5F(0)$, and thus L_ϕ is

estimated by $L_\phi = (2.4h/eB_0)^{1/2}$ (Ref. [27]). The estimated $L_\phi(T = 1.5$ K) ~ 253 nm is much larger than the nanowire diameter D , suggesting a quasi-one-dimensional (1D) phase-coherent transport. The estimated L_ϕ is also consistent with that obtained from the WAL effect [17,23]. As shown in Fig. 3(b), the δG_B^{rms} decays with increasing temperature in a $T^{-3/4}$ power-law manner, in well agreement with the quasi-1D transport model, that $\delta G_B^{rms} = (e^2/h)(L_\phi/L)^{3/2}$ and $L_\phi \propto T^{-1/2}$ (Ref. [25]).

As aforementioned, the UCF pattern has a close dependence on the position of Fermi-level E_F . Figure 4(a) shows the conductance fluctuation δG as a function of B at various gate voltages and at 1.5 K. Clearly, the UCF pattern δG differs from each other in both shape and magnitude at different gate voltages. As shown in Fig. 4(b), the $\delta G_B^{rms} = 0.129e^2/h$ at $V_g = 100$ V is more than 20 times larger than $\delta G_B^{rms} = 0.0064e^2/h$ at $V_g = 20$ V, whereas the ratio of $G(V_g = 100$ V)/ $G(V_g = 20$ V) is merely ~ 3.3 . Because $\delta G_B^{rms} \propto (L_\phi/L)^{3/2}$ for the 1D system, the V_g dependence of L_ϕ is responsible for the gate-voltage-dependent conductance fluctuations. From the autocorrelation function $F(\Delta B)$, L_ϕ is extracted and presented in Fig. 4(c). For $V_g < 20$ V, the impact of vacancies on the scatterings in the valence band can strongly reduce the coherence length L_ϕ (Ref. [12]).

It is worth noting that L_ϕ reaches the minimum value at the Dirac point $V_g = 20$ V and increases by a factor of ~ 3 from $V_g = 20$ to 100 V. Because the nanowire is grown along the [110] direction, the perpendicular magnetic field should be on the (110) plane. Theory predicts that the rotational

symmetry-protected Dirac point will be lifted by applying a magnetic field deviating from the [001] direction of the Cd_3As_2 crystal [2,3,12]. Therefore, the opening of a band gap near the Dirac point will reduce the Fermi velocity and generate a mass of the Dirac fermions, which results in the decrease in carrier mobility and thus L_ϕ . To reveal the generation of the field-induced gap, we concentrate on how the external field affects the temperature dependence of the resistance as shown in Fig. 4(d). It is found that the R - T dependence is transformed from a metallic behavior under $B = 0$ T to an insulating behavior under $B = 14$ T at temperatures below 6 K. This field-induced transition has also been observed in plenty of gapless materials [8,28–30], giving evidence for the gap opening at the band crossing point.

To explore the influence of the magnetic-field-induced symmetry breaking on the phase-coherent transport, we measured the gate-voltage-dependent conductance fluctuations δG of a typical device with short-channel $L \sim 180$ nm and nanowire diameter of $D \sim 130$ nm under different magnetic fields. The transfer curve shows the Dirac point of this device is about 5 V [Fig. 5(a)]. As shown in Fig. 5(b), the conductance fluctuations are much more prominent in the electron branch than those in the hole branch. Moreover, it is found that application of a magnetic field reduces the amplitude of fluctuations significantly. To be quantitative, we calculate the δG^{rms} at two distinct regimes of Fermi-level E_F : One is around the Dirac point ($V_g : 0$ –15 V), and the other is far away from the Dirac point ($V_g : 20$ –50 V). As shown in Fig. 5(c), the normalized amplitude $\delta G^{rms}(B)/\delta G^{rms}(B = 0$ T) decreases markedly by increasing the magnetic field B to 2 T and then tends to saturate up to $B = 8$ T, irrespective of the doping level. This unusual saturation reminds us of the random-matrix theory (RMT) that well explains the reduction of the UCF in graphene, a quantum dot, and a two-dimensional electron gas system in the presence of a magnetic field [22,26,31]. The conductance fluctuations are sensitive to the configuration of impurity related to the transfer matrix in the Landauer-Büttiker formula [32]. To study all the impurity configurations statistically, one prevailing treatment, namely, the RMT is to map all the possible configurations by a set of random transfer matrices [32]. The amplitude of the UCF has a relation with the symmetry of the random-matrix ensemble in $\delta G^{rms} \sim (e^2/h)s\sqrt{\frac{k}{\beta}}$, where k is the number of independent eigenvalue sequences of the Hamiltonian, s is the eigenvalue degeneracy, and β is 4, 2, and 1 for the Gaussian symplectic ensemble (GSE), the Gaussian unitary ensemble (GUE), and the orthogonal ensemble, respectively [30]. In Dirac semimetals, the total degeneracy s is determined by spin degeneracy $v_s = 2$, orbital-related (overlapping Weyl nodes) degeneracy $v_p = 2$, and Kramers degeneracy $v_K = 2$, yielding $s = 8$ in the absence of a magnetic field. Meanwhile, the so-called GSE system has $\beta = 4$ as a consequence of spin-orbit interaction and preservation of time-reversal symmetry. Application of a magnetic field $B > B_C = \frac{\phi_0}{L \times W} \sim 88$ mT ($L, W < L_\phi$) causes a transition from GSE to GUE ($\beta = 2$), accompanied by the reduction of v_p and v_k to 1. The transition from $v_p = 2$ to $v_p = 1$ results from the splitting of overlapped Weyl points due to the breaking of time-reversal symmetry. Consequently, the ratio of $\delta G^{rms}(B > B_C)/\delta G^{rms}(B = 0$ T) is expected to be

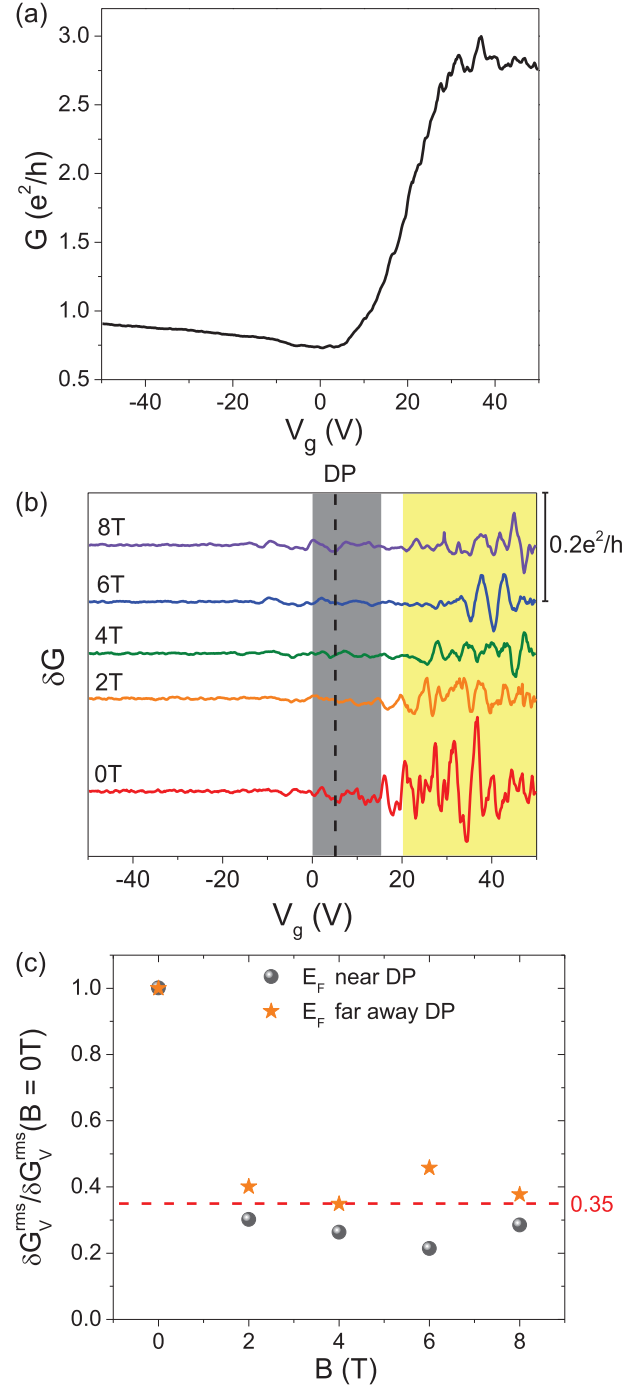


FIG. 5. Gate-voltage dependence of a device with short-channel ~ 180 nm at 1.5 K. (a) Transfer curve of the device, showing the location of the Dirac point is ~ 5 V. (b) Extracted fluctuations δG at different magnetic fields $B = 0, 2, 4, 6,$ and 8 T. (c) Normalized δG_V^{rms} by $\delta G_V^{rms}(B = 0$ T) as a function of the magnetic field as the Fermi level is close to (gray ball) or far away from (orange star) the Dirac point.

$\frac{1}{2\sqrt{2}} \sim 0.35$ and saturates by further increasing the magnitude of the magnetic field, which is well in agreement with the results in Fig. 5(c). Even in the highly doping regime at $V_g = 50$ V, the Fermi-level $E_F \sim 89$ meV is still far from the Lifshitz transition point located at ~ 200 meV (Ref. [12]),

preserving the consistency of transport properties during gate modulation.

To summarize, we have demonstrated the UCFs in Dirac semimetal Cd_3As_2 nanowires. The magnitude of the UCF has a power-law decay of $\sim T^{-3/4}$ with temperature T indicating its quasi-1D nature. The gate-modulation experiments reveal the strong suppression of the UCF at the Dirac point, which is ascribed to the band-gap opening at the Dirac point due to the magnetic-field-induced rotational symmetry breaking. Furthermore, the splitting of the Dirac point into two Weyl nodes by the breaking of time-reversal symmetry under a magnetic field can result in the reduction of the UCF's

amplitude by a factor of $\sim 2\sqrt{2}$. These findings are helpful for understanding the phase-coherent ($L < L_\phi$) transport in 3D Dirac semimetals as the device size down to the nanoscale. Our results may be valuable for studying 3D massive fermions and exotic topological phases in Dirac semimetals with band-gap openings.

This work was supported by National Key Research and Development Program of China (Grants No. 2016YFA0300802, No. 2013CB934600, and No. 2013CB932602) and National Natural Science Foundation of China (Grants No. 11274014 and No. 11234001).

-
- [1] S. M. Young, S. Zaheer, J. C. Y. Teo, C. L. Kane, E. J. Mele, and A. M. Rappe, *Phys. Rev. Lett.* **108**, 140405 (2012).
- [2] Z. Wang, H. Weng, Q. Wu, X. Dai, and Z. Fang, *Phys. Rev. B* **88**, 125427 (2013).
- [3] Z. Wang, Y. Sun, X.-Q. Chen, C. Franchini, G. Xu, H. Weng, X. Dai, and Z. Fang, *Phys. Rev. B* **85**, 195320 (2012).
- [4] Z. K. Liu *et al.*, *Science* **343**, 864 (2014).
- [5] Z. K. Liu *et al.*, *Nature Mater.* **13**, 677 (2014).
- [6] M. Neupane *et al.*, *Nat. Commun.* **5**, 3786 (2014).
- [7] S. Borisenko, Q. Gibson, D. Evtushinsky, V. Zabolotnyy, B. Büchner, and R. J. Cava, *Phys. Rev. Lett.* **113**, 027603 (2014).
- [8] T. Liang, Q. Gibson, M. N. Ali, M. Liu, R. J. Cava, and N. P. Ong, *Nature Mater.* **14**, 280 (2014).
- [9] Y. Zhao, H. Liu, C. Zhang, H. Wang, J. Wang, Z. Lin, Y. Xing, H. Lu, J. Liu, Y. Wang, S. M. Brombosz, Z. Xiao, S. Jia, X. C. Xie, and J. Wang, *Phys. Rev. X* **5**, 031037 (2015).
- [10] S. A. Parameswaran, T. Grover, D. A. Abanin, D. A. Pesin, and A. Vishwanath, *Phys. Rev. X* **4**, 031035 (2014).
- [11] Y. Xiang *et al.*, *arXiv:1601.02316*.
- [12] S. Jeon, B. B. Zhou, A. Gyenis, B. E. Feldman, I. Kimchi, A. C. Potter, Q. D. Gibson, R. J. Cava, A. Vishwanath, and A. Yazdani, *Nature Mater.* **13**, 851 (2014).
- [13] I. Zeljkovic *et al.*, *Nature Mater.* **14**, 318 (2014).
- [14] L. P. He, X. C. Hong, J. K. Dong, J. Pan, Z. Zhang, J. Zhang, and S. Y. Li, *Phys. Rev. Lett.* **113**, 246402 (2014).
- [15] J. Cao *et al.*, *Nat. Commun.* **6**, 6779 (2015).
- [16] Z. J. Xiang, D. Zhao, Z. Jin, C. Shang, L. K. Ma, G. J. Ye, B. Lei, T. Wu, Z. C. Xia, and X. H. Chen, *Phys. Rev. Lett.* **115**, 226401 (2015).
- [17] C.-Z. Li, L.-X. Wang, H. Liu, J. Wang, Z.-M. Liao, and D.-P. Yu, *Nat. Commun.* **6**, 10137 (2015).
- [18] H. Li, H. He, H. Z. Lu, H. Zhang, H. Liu, R. Ma, Z. Fan, S. Q. Shen, and J. Wang, *Nat. Commun.* **7**, 10301 (2016).
- [19] C. Zhang *et al.*, *arXiv:1504.07698*.
- [20] J. Xiong, S. K. Kushwaha, T. Liang, J. W. Krizan, M. Hirschberger, W. Wang, R. J. Cava, and N. P. Ong, *Science* **350**, 413 (2015).
- [21] L. A. Jauregui, M. T. Pettes, L. P. Rokhinson, L. Shi, and Y. P. Chen, *Nat. Nanotechnol.* **11**, 345 (2016).
- [22] A. N. Pal, V. Kochat, and A. Ghosh, *Phys. Rev. Lett.* **109**, 196601 (2012).
- [23] B. Zhao, P. Cheng, H. Pan, S. Zhang, B. Wang, G. Wang, F. Xiu, and F. Song, *Sci. Rep.* **6**, 22377 (2016).
- [24] L.-X. Wang, C.-Z. Li, D.-P. Yu, and Z.-M. Liao, *Nat. Commun.* **7**, 10769 (2016).
- [25] L. Vila, R. Giraud, L. Thevenard, A. Lemaitre, F. Pierre, J. Dufouleur, D. Mailly, B. Barbara, and G. Faini, *Phys. Rev. Lett.* **98**, 027204 (2007).
- [26] P. Debray, J.-L. Pichard, J. Vicente, and P. N. Tung, *Phys. Rev. Lett.* **63**, 2264 (1989).
- [27] Y.-F. Chen, M.-H. Bae, C. Chialvo, T. Dirks, A. Bezryadin, and N. Mason, *J. Phys.: Condens. Matter* **22**, 205301 (2010).
- [28] C. Shekhar *et al.*, *Nat. Phys.* **11**, 645 (2015).
- [29] M. N. Ali *et al.*, *Nature (London)* **514**, 205 (2014).
- [30] X. Du, S.-W. Tsai, D. L. Maslov, and A. F. Hebard, *Phys. Rev. Lett.* **94**, 166601 (2005).
- [31] J. A. Folk, S. R. Patel, K. M. Birnbaum, C. M. Marcus, C. I. Duruoaz, and J. S. Harris, *Phys. Rev. Lett.* **86**, 2102 (2001).
- [32] K. A. Muttalib, J.-L. Pichard, and A. D. Stone, *Phys. Rev. Lett.* **59**, 2475 (1987).